A LETTERS JOURNAL EXPLORING THE FRONTIERS OF PHYSICS

OFFPRINT

Tight-binding normal mode analysis of suspended single-wall carbon nanotubes

T. A. Beu and A. Farcaş

EPL, **113** (2016) 37004

OVER
560,000
full text downloads in 2013

24 DAYS
average accept to online publication in 2013

10,755
citations in 2013

"We greatly appreciate the efficient, professional and rapid processing of our paper by your team."

Cong Lin
Shanghai University

Six good reasons to publish with EPL

We want to work with you to gain recognition for your research through worldwide visibility and high citations. As an EPL author, you will benefit from:

1. **Quality** – The 50+ Co-editors, who are experts in their field, oversee the entire peer-review process, from selection of the referees to making all final acceptance decisions.
2. **Convenience** – Easy to access compilations of recent articles in specific narrow fields available on the website.
3. **Speed of processing** – We aim to provide you with a quick and efficient service; the median time from submission to online publication is under 100 days.
4. **High visibility** – Strong promotion and visibility through material available at over 300 events annually, distributed via e-mail, and targeted mailshot newsletters.
5. **International reach** – Over 2600 institutions have access to EPL, enabling your work to be read by your peers in 90 countries.
6. **Open access** – Articles are offered open access for a one-off author payment; green open access on all others with a 12-month embargo.

Details on preparing, submitting and tracking the progress of your manuscript from submission to acceptance are available on the EPL submission website **www.epletters.net**.

If you would like further information about our author service or EPL in general, please visit **www.epljournal.org** or e-mail us at **info@epljournal.org**.

EPL is published in partnership with:

European Physical Society | Società Italiana di Fisica | EDP Sciences | IOP Publishing

A Letters Journal Exploring the Frontiers of Physics

February 2016

EPL, **113** (2016) 37004
doi: 10.1209/0295-5075/113/37004

www.epljournal.org

Tight-binding normal mode analysis of suspended single-wall carbon nanotubes

T. A. Beu[(a)] and A. Farcaş

University "Babeş-Bolyai", Faculty of Physics, Department of Biomolecular Physics - 400084 Cluj-Napoca, Romania

received 3 December 2015; accepted in final form 13 February 2016
published online 25 February 2016

PACS 71.15.Nc – Total energy and cohesive energy calculations
PACS 78.20.Bh – Theory, models, and numerical simulation
PACS 78.30.Na – Fullerenes and related materials

Abstract – We present a detailed normal mode analysis of suspended single-wall carbon nanotubes based on a non-orthogonal tight-binding formalism and a new methodology for classifying vibrational modes, using geometry-adapted merit functions. The fundamental modes are in good agreement with experiments and previous calculations. The analysis of the high-order vibrations evidences interesting non-classical features, while the sensitivity of the normal modes to the nanotube geometry provides new insights useful for practical realizations of mass resonators.

Introduction. – Carbon nanotubes (CNTs) have been demonstrated to be ideally suited for topical nano-electromechanical applications [1–6]. CNTs can accommodate high-frequency natural vibrations with high-quality factors, and, given their extreme sensitivity to external perturbations, the shifts of the resonance frequencies can be used to accurately measure supplementary masses attached to the CNTs. In fact, the nanomechanical mass sensor reported by Jensen *et al.* [2] attained a remarkable sensitivity of the order of $10^{-25}\,\mathrm{kg}\cdot\mathrm{Hz}^{-1/2}$.

The detailed knowledge of the natural vibrations of CNTs under various suspension conditions remains essential for developing enhanced setups for CNT-based mass resonators. The diameter-selective Raman scattering studies of Rao *et al.* [7] on single-wall CNTs have evidenced radial, breathing, and scissoring modes, while the complementary normal mode analysis, based on force constants and periodic boundary conditions, has fairly explained the measured Raman spectra.

The theoretical investigations published so far essentially fall into three categories. a) *Normal mode analysis* methodologies based on the eigenvalue problem of the dynamical (Hessian) matrix, constructed either using force constants [7,8] or tight-binding force fields [9]. While in [7,9] the applied periodic boundary conditions implicitly model free (non-suspended) CNTs of infinite length, in [8] time-averaged Hessians for finite CNTs are used. b) *Molecular dynamics simulations* using interatomic potentials and Fourier-transformed correlation functions to extract the vibrational spectrum [10–13]. As an inherent limitation, this approach does not equally provide the atomic displacements to completely characterize the normal modes. c) *Continuum beam models* based on the Euler-Bernoulli or Timoshenko equations [11–16]. Even though the Timoshenko model incorporates corrections for shear deformation and rotary inertia, it is yet limited to classical modes not involving structural atomistic particularities. Nevertheless, recent MD simulations using the Brenner potential [10,12,13] confirm the applicability of carefully parametrized Timoshenko beam models for the lowest flexural vibrational modes of suspended CNTs.

In this paper we present a detailed first-principles normal mode analysis of suspended single-wall CNTs, extended up to high modes. The electronic structures are calculated in the framework of a non-orthogonal tight-binding (TB) formalism, and the normal mode analysis is based on the eigenvalue problem of the Hessian matrix. We consider armchair-type CNTs clamped at both ends (CC), or with one end free (CF). To cope with the considerable complexity of the high-order normal modes, a general methodology based on specialized merit functions is devised to automate the disambiguation of the vibrations. The in-depth analysis of the sensitivity of the various normal modes to the geometric features of the CNTs enables new insights and provides clues for efficient practical realizations of mass resonators. As a noteworthy advantage over previous studies, besides consistently relying on first-principles electronic structures, our approach provides the

(a) E-mail: titus.beu@phys.ubbcluj.ro

complete normal mode analysis including atomic displacement patterns. Moreover, the novel methodology for classifying vibrations up to arbitrary orders is transferable to other force fields.

Non-orthogonal tight-binding formalism. – The non-orthogonal TB parametrization of Papaconstantopoulos *et al.* [17], which we have extensively used in several structural and vibrational studies on fullerenes [18–21], assigns a pseudo-atomic density to each atom i:

$$\rho_i = \sum_{j\neq i}^{N} e^{-\lambda^2 R_{ij}} f(R_{ij}), \quad i,j = 1,N, \tag{1}$$

which depends exponentially on the distances to all neighbors with a cutoff $f(R) = \{1+\exp[(R-R_c)/\Delta\}^{-1}$. The local density determines the diagonal *on-site* Hamiltonian elements,

$$h_l^i = \alpha_l + \beta_l \rho_i^{2/3} + \gamma_l \rho_i^{4/3} + \chi_l \rho_i^2, \qquad l = s,p, \tag{2}$$

while the *hopping parameters* are defined as ($\mu = \sigma, \pi$):

$$H_{ll'\mu}(R) = (a_{ll'\mu} + b_{ll'\mu}R + c_{ll'\mu}R^2)e^{-d^2_{ll'\mu}R} f(R), \tag{3}$$

$$S_{ll'\mu}(R) = (\delta_{ll'} + p_{ll'\mu}R + q_{ll'\mu}R^2 + r_{ll'\mu}R^3)e^{-s^2_{ll'\mu}R} f(R). \tag{4}$$

The non-diagonal elements of the Hamiltonian matrix **H** and overlap matrix **S** are expressed in terms of these hopping parameters and bond direction cosines.

The normal mode analysis for the fully relaxed molecular system is performed within the harmonic approximation, using the Hessian matrix,

$$\mathcal{H}_{ij}^{\alpha\beta} = \partial F_i^\alpha / \partial R_j^\beta, \quad i,j = 1,N, \quad \alpha,\beta = x,y,z, \tag{5}$$

where R_i^α is the α-component of the position vector of atom i, and F_i^α, the corresponding force component. The resonance vibrations are determined by solving the eigenvalue problem:

$$\mathcal{H}\cdot\delta\mathbf{r}_k = \omega_k^2 \mathbf{M}\cdot\delta\mathbf{r}_k, \qquad k = 1,3N, \tag{6}$$

where **M** is the diagonal matrix of atomic masses, ω_k is the eigenfrequency of the normal mode k, and the components of the eigenvector $\delta\mathbf{r}_k$ are the corresponding atomic displacements.

Merit functions. – Based on the predominant direction of the atomic displacements, we conventionally distinguish *radial*, *axial*, and *twisting* normal modes. Technically, we consider armchair-type CNTs aligned about the z-axis and subdivide them into equal transversal slices Δ_z, each enclosing only C atoms with identical z-coordinates. Denoting by $(\delta x_i, \delta y_i, \delta z_i)$ the displacement components of atom i for a given mode, $\delta r_i = (x_i\cdot\delta x_i + y_i\cdot\delta y_i)/\sqrt{x_i^2+y_i^2}$ is the radial displacement.

To characterize predominantly radial vibrations, we model the envelope of the radial displacement patterns

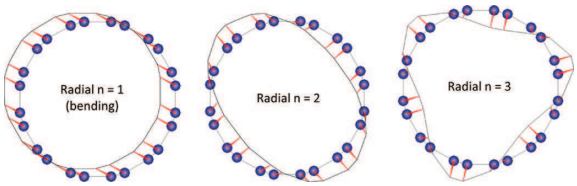

Fig. 1: (Color online) Atomic displacement patterns in the central transversal plane of a CC (6,6) CNT for the fundamental radial modes of orders $n = 1,2,3$. Continuous line: the displacement profile modeled by the merit functions.

in a transversal plane by periodic dependences ($\cos n\varphi$) of various orders $n = 0,1,\ldots$ on the polar atomic positions. From this unifying perspective, the symmetric breathing and bending modes are, respectively, 0th- and 1st-order radial modes (fig. 1). Based on the periodic model functions of various orders, we define the set of merit functions:

$$F_r^n = 1 - \sum_{\Delta_z}\sum_{i\in\Delta_z} \left|\cos n\varphi_i - \delta r_i/\delta r_{\max}\right|, \tag{7}$$

where φ_i is the polar angle between atom i and the atom featuring the maximum radial displacement $\delta r_{\max}$ within the considered slice Δ_z, and $\sum_{\Delta_z}$ designates the summation over all slices of a CNT. Clearly, F_r^0 is maximized for symmetric radial modes, while F_r^1, for bending vibrations.

By analogy, axial vibrations are characterized by a set of merit functions based on periodic model functions for the axial displacement patterns:

$$F_z^n = 1 - \sum_{\Delta_z}\sum_{i\in\Delta_z} \left|\cos n\varphi_i - \delta z_i/\delta z_{\max}\right|, \tag{8}$$

where φ_i is the polar angle between atom i and the atom featuring the maximum axial displacement $\delta z_{\max}$ within the considered slice Δ_z. Obviously, F_z^0 is maximized for stretching, while F_z^1, for axial scissoring.

The merit function maximized for twisting modes cumulates the (axial) vector products of the transversal displacements and the radial atomic positions in each slice, and sums up the corresponding absolute values (accounting for the fact that for higher harmonics, different slices may twist in anti-phase):

$$F_t = \sum_{\Delta_z}\left|\sum_{i\in\Delta_z}(x_i\cdot\delta y_i - y_i\cdot\delta x_i)\right|. \tag{9}$$

Each type of merit function is normalized separately by the division to the maximum attained for a given CNT.

Classifying a particular normal mode proceeds by first checking for a maximal value of F_t, the case in which a twisting mode is identified. As a second step, a gross initial distinction between radial and axial modes is made based on the ratio of the overall radial to axial displacements:

$$\chi = \sum_{\Delta_z}\sum_{i\in\Delta_z}|\delta r_i| \Big/ \sum_{\Delta_z}\sum_{i\in\Delta_z}|\delta z_i|. \tag{10}$$

Table 1: Synthetic structural features of the considered CNTs.

Chirality	Length (rings)	No. of atoms	E_{gap} (eV)	E_{bind} (eV)
(5,5)	15	320	0.184	10.10
	40	820	0.135	10.17
(6,6)	18	456	0.099	10.18
	40	984	0.036	10.22
(7,7)	21	616	0.062	10.20
	40	1148	0.010	10.25

A value $\chi \geq 1$ defines a radial mode, while $\chi < 1$ defines an axial mode. The actual order n of the identified radial/axial vibration is finally determined by the maximum of the F_r^n or, respectively, F_z^n values.

Results and discussion. – We focus our investigations on armchair-type single-wall CNTs of chiralities (5,5), (6,6), and (7,7), and lengths ranging between 3.70 and 9.88 nm. Their limiting geometric and electronic features are listed in table 1. The aspect ratios are confined to ranges exceeding 5.4, a value below which the distinction of the normal modes becomes increasingly difficult.

The equilibrium structures of the CNTs are obtained by simulated annealing in molecular dynamics runs spanning 1 ns of simulation time with a time step of 1 fs. The relaxation causes slight deformations of the CNT ends, however preserving the inversion points for odd-valued chiralities. As expected for the conducting armchair-type CNTs, the HOMO-LUMO gap reduces both with increasing CNT length and chirality, while the stability, as indicated by the binding energy per atom, E_{bind}, slightly increases.

Illustrating characteristic displacement patterns, figs. 2(a) to (e) depict the second harmonics for selected radial, twisting, and axial vibrations, in increasing order of their resonance frequencies: bending (radial 1), breathing (radial 2), twisting, stretching (axial 0), and scissoring (axial 1) (see the corresponding supplementary animated images `Fig2a.gif`, `Fig2b.gif`, `Fig2c.gif`, `Fig2d.gif` and `Fig2e.gif`). For ease of viewing, only the displacements in the semi-cylindrical upper half of the nanotube are shown. Apart from the symmetric radial (radial 0), stretching, and twisting vibrations, the rest of the radial/axial modes are doubly degenerate. Excepting the bending modes, the resonance vibrations of the CNTs are Raman active.

Figures 3(a) and (b) emphasize an interesting feature defining the radial 0 and axial 0 vibrations of suspended CNTs —their invariable coupling (see the corresponding supplementary animated images `Fig3a.gif` and `Fig3b.gif`). Axial regions with predominantly axial displacements are seen to enclose regions dominated by radial displacements, and the vibrations correspond at the same time to well-defined axial and radial harmonics. While

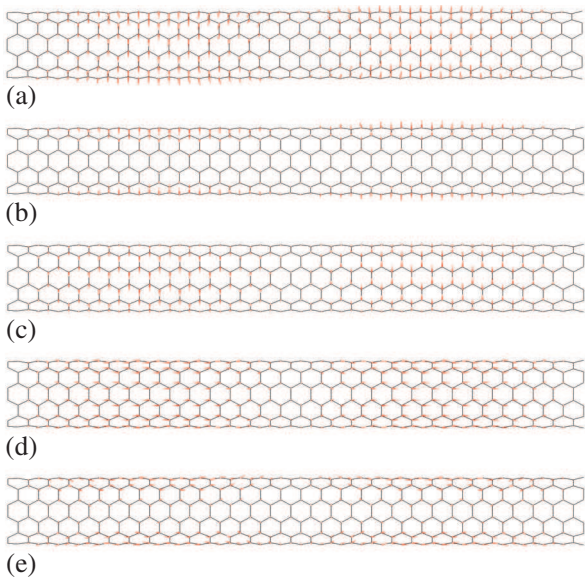

Fig. 2: (Color online) Atomic displacements for selected second harmonics in a side view of a CC (6,6) CNT (28 rings in length): (a) radial 1 (bending) at 0.97 THz, (b) radial 2 (breathing) at 1.54 THz, (c) twisting at 2.15 THz, (d) axial 0 (stretching) at 3.27 THz, and (e) axial 1 (scissoring) at 6.41 THz.

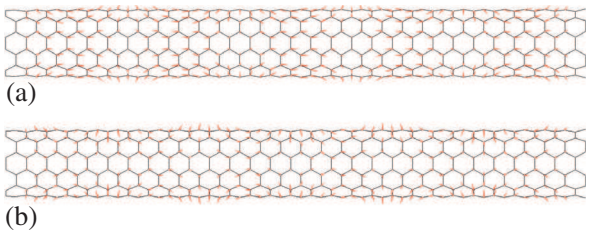

Fig. 3: (Color online) Mixing of the radial 0 and axial 0 modes in a CC (6,6) CNT: (a) the 5th axial 0 (4th radial 0) harmonic at 7.61 THz, with dominant axial character ($\chi = 0.7$). (b) the 6th axial 0 (5th radial 0) harmonic at 8.26 THz with dominant radial character ($\chi = 1.6$).

for lower frequencies the axial character dominates overall these mixed harmonics (as indicated by $\chi < 1$), preventing the low radial harmonics to be identified as such, with increasing resonance frequencies the radial character starts prevailing ($\chi > 1$) and the axial modes go over into radial ones.

For low harmonics, the assignment of a well-defined vibrational character is straightforward, and, as a clear quantitative indication, a single merit function copiously dominates the others. For high harmonics or high radial/axial mode orders, however, the vibrations become increasingly intricate, featuring a rather mixed character, reflected by significant values of several merit functions. Disambiguation is particularly challenging in frequency regions where high harmonics of low-order radial/axial vibrations coexist with the dominating fundamental harmonics of higher-order modes.

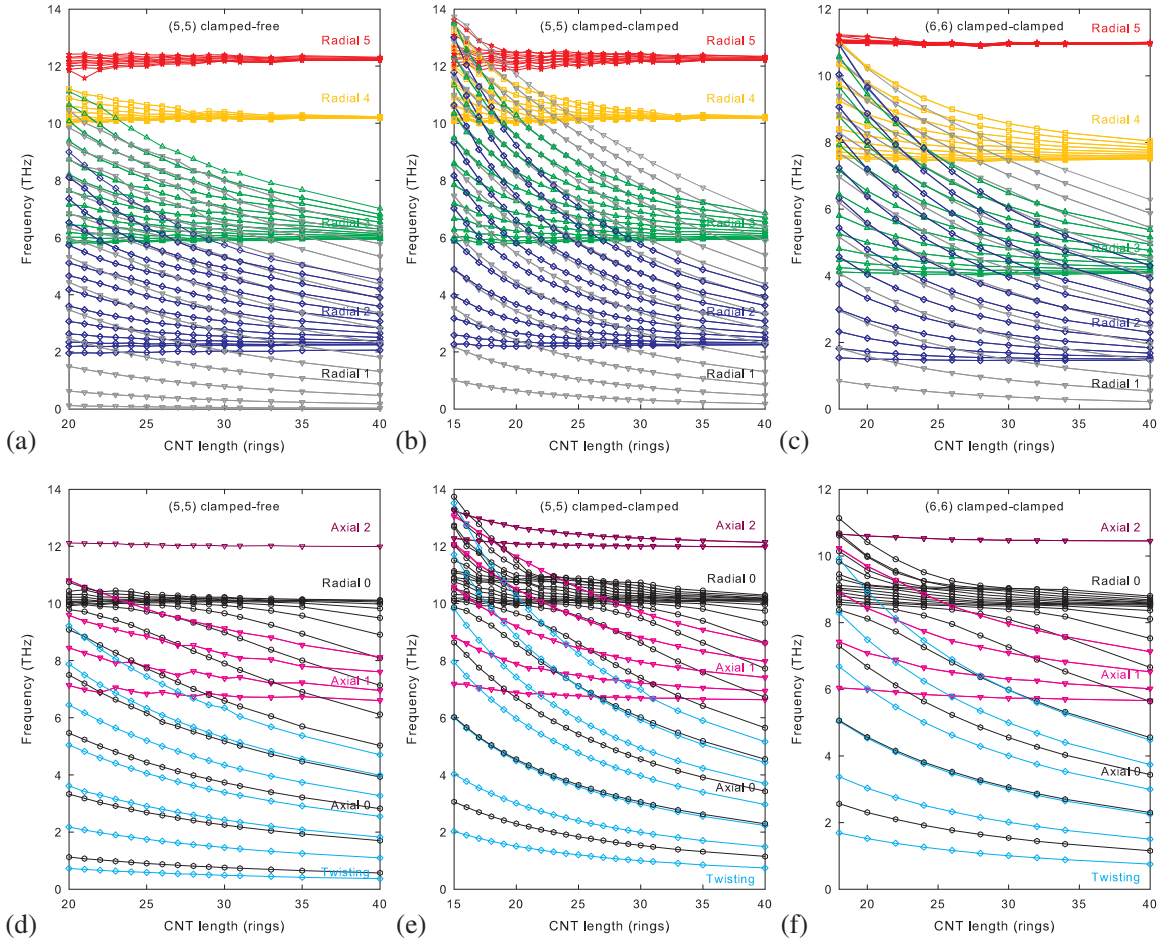

Fig. 4: (Color online) CNT length dependence of the frequencies for the lowest 150 normal modes of (5,5) and (6,6) CNTs. Radial modes ($n = 1$ to 5) of (a) CF (5,5), (b) CC (5,5), and (c) CC (6,6) CNTs. Axial, twisting, and radial 0 modes of (d) CF (5,5), (e) CC (5,5), and (f) CC (6,6) CNTs.

Figures 4(a) to (f) comparatively illustrate the CNT length dependence of the resonance frequencies for the lowest 150 normal modes of the (5,5) and (6,6) CNTs. The figures of the upper row (figs. 4(a) to (c)) correspond to the radial modes of orders 1 to 5, while those of the lower row (figs. 4(d) to (f)) represent the axial and twisting vibrations. The plots on the left correspond to CF (5,5) CNTs, the central ones, to CC (5,5) CNTs, and those on the right, to CC (6,6) CNTs.

Except for the systematically lower frequencies, the overall patterns of the resonance curves for the (6,6) CNTs are essentially similar to those for the (5,5) CNTs, and the frequency lowering tendency is continued for the (7,7) CNTs. The similarity between the resonance curves of CC and CF CNTs of the same chirality is also apparent.

The fundamental harmonics of the various types of normal modes define a system of well-separated, weekly varying levels. In the limit of the longest CNTs considered (98.8 Å), the practically unvarying fundamental frequencies can be assimilated with those of macroscopically long CNTs. The entire system of fundamentals and associated harmonics for the radial and, respectively, axial modes is seen to be organized in ascending order of the vibration orders (radial 1, radial 2, etc., and, respectively, axial 0, axial 1, etc.). The occurrence of the radial 0 (symmetric breathing) modes only at rather high frequencies, above 8 THz (figs. 4(d) to (f)), would appear to indicate them as exceptions to the overall monotonic order-wise ordering. In fact, as already pointed out in regard to figs. 3(a) and (b), the axial 0 and radial 0 harmonics coexist strongly coupled, with the dominant character of the successive harmonics gradually changing from axial to radial. In other words, the low radial harmonics are not actually identified since they are overwhelmed by the axial behavior manifested in their nodal regions, and the vibrations are rather assigned an axial overall character. Moreover, the resonance curves for the axial 0 and radial 0 vibrations also depart in their transition region from the qualitative inverse CNT length dependences observed for other normal modes.

Aside from the generally similar frequency curve patterns, the supplementary lower axial and twisting harmonics occurring for the CF CNTs can be set in one-to-one correspondences with resonances of CC CNTs of

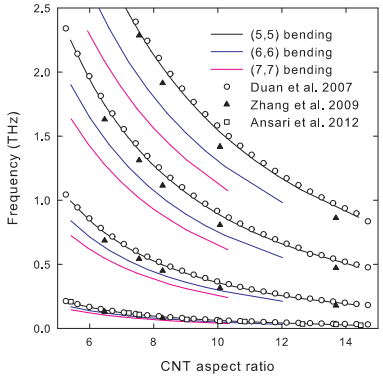

Fig. 5: (Color online) CNT aspect ratio dependence of the frequencies of the lowest four CF bending (radial 1) modes, along with published MD results [10–12].

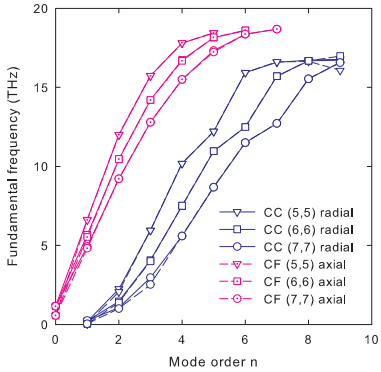

Fig. 6: (Color online) Dependence of the extrapolated fundamental frequencies of the radial/axial modes on the mode order.

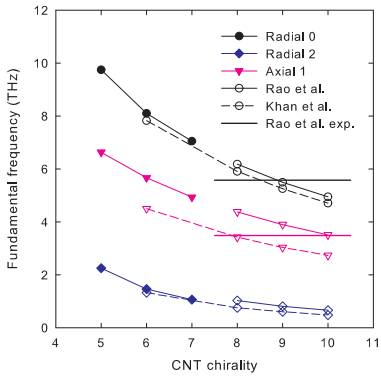

Fig. 7: (Color online) Comparison of the extrapolated fundamental frequencies (filled symbols) with the experiments and force constant-based calculations of Rao *et al.* [7] (continuous lines and empty symbols), and with the TB calculations of Kahn *et al.* [9] (dashed lines and empty symbols).

double length. Such correlations can be readily checked, for instance, for the twisting fundamentals of the CC CNT of 40 rings in length (fig. 4(f)) and the CF CNT of half length (fig. 4(d)), or for the axial 0 fundamentals of the same pair of CNTs. Noteworthy, the CF profiles are less smooth than their CC counterparts, reflecting a somewhat less well-defined character of the CF normal modes. This aspect becomes increasingly significant for CNTs of lower aspect ratio, which, alongside the growing perturbing influence of the ends, is the reason for which we did not consider CF CNTs of aspect ratios below 5.4.

Normal modes different in nature incidentally show similar CNT length dependence, irrespective of chirality. For example, the 2nd axial 0 harmonic and the 3rd twisting harmonic run almost overlapped for all CC CNTs over the entire range of lengths.

Figure 5 comparatively shows the frequencies of the four lowest bending modes of the CF (5,5), (6,6), and (7,7) CNTs as functions of the aspect ratio. While the fundamental harmonics show a relatively reduced dependence on the chirality, the differences gradually grow for the higher harmonics, with the (5,5) CNTs featuring, as expected, the higher frequencies. The MD studies of Duan *et al.* [11], based on the COMPASS force field, have resulted in resonance frequencies for the four lowest modes of (5,5) CNTs in fair agreement with our lowest *bending* harmonics. The resonance curves of Zhang *et al.* [12] and Ansari *et al.* [10], based on the Brenner potential, fall slightly lower than our dependences, suggesting somewhat softer C-C bonding.

The fundamental frequencies of the radial and axial modes increase monotonically as functions of the mode order (fig. 6), however, saturating at about 17 THz and 19 THz, respectively. These two well-separated levels benefit from little sensitivity both to CNT length and chirality, or, in practical terms, to structural inaccuracies. Understandably, the monotonic increase for the radial modes is slightly perturbed for mode orders matching the chiral indexes (5, 6, and, respectively, 7), while the axial modes are insensitive, producing smooth dependences.

The CNT chirality dependences of the extrapolated fundamental harmonics for the radial 0 (symmetric radial), radial 2 (breathing), and axial 1 (scissoring) modes (fig. 7) show consistency with the resonance frequencies calculated by Rao *et al.* [7] for infinitely long CNTs of larger chiralities ((8,8) to (10,10)). Our results are bounded below by their experimental frequencies (horizontal lines), which have been though obtained for mixtures of CNTs with chiral indexes ranging from 8 to 10. In addition, the above analysis on the coupling of the axial 0 and radial 0 modes explains the experimental observation of the symmetric radial mode at a higher frequency than the fundamental scissoring mode. In turn, the TB frequencies calculated by Khan *et al.* [9] show a systematic underestimation tendency, especially for the axial mode.

The resonance frequencies for the twisting and stretching modes appear to be chirality independent (fig. 8(a)), being therefore potentially useful for practical realizations of mass resonators. Notably, the frequencies for CC CNTs (with continuous lines) are the doubles of their CF counterparts. Quite in contrast, the behavior of the radial and

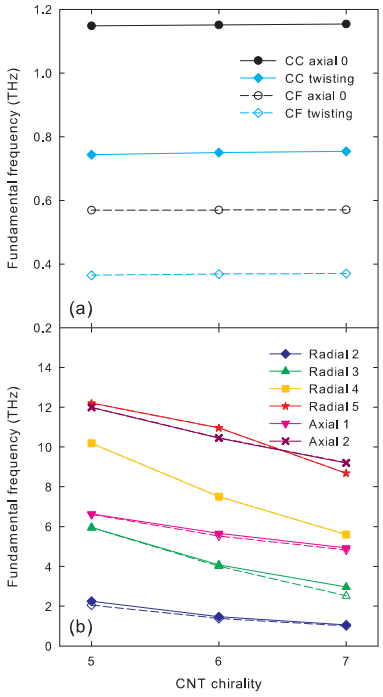

Fig. 8: (Color online) CNT chirality dependence of the extrapolated fundamental frequencies for: (a) axial 0 (stretching) and twisting, and (b) radial (1 to 5) and axial (1 and 2) modes.

scissoring modes, even though chirality dependent, is similar for CC and CF CNTs (fig. 8(b)).

Conclusions. – We report a detailed normal mode analysis of clamped-clamped and clamped-free CNTs based on a non-orthogonal tight-binding force field, and a novel methodology using geometry-adapted merit functions for characterizing vibrations up to high orders.

While the low harmonics are simple and intuitive, featuring continuum analogs, high harmonics tend to mix and are rather complex. The extrapolated fundamental frequencies are consistent with experiments and previous calculations based on force constants. The low bending vibrations are also found in fair agreement with continuum theory results. The extrapolated fundamental frequencies for twisting and stretching are essentially chirality independent, being therefore useful for practical realizations of mass resonators.

The presented calculations fill a gap in the literature, extending the range of the vibrational analysis up to high orders, while the developed merit-function–based methodology enables accurate predictions for sizeable CNTs in conjunction with arbitrary force fields.

REFERENCES

[1] Sazonova V., Yaish Y., Ustunel H., Roundy D., Arias T. A. and McEuen P. L., *Nature (London)*, **431** (2004) 284.
[2] Jensen K., Kim K. and Zettl A., *Nat. Nanotechnol.*, **3** (2008) 553.
[3] Eichler A., Moser J., Chaste J., Zdrojek M., Wilson-Rae I. and Bachtold A., *Nat. Nanotechnol.*, **6** (2011) 339.
[4] Chaste J., Eichler A., Moser J., Ceballos G., Rurali R. and Bachtold A., *Nat. Nanotechnol.*, **7** (2012) 301.
[5] Laird E., Pei F., Tang W., Steele G. and Kouwenhoven L., *Nano Lett.*, **12** (2012) 193.
[6] Island J., Tayari V., McRae A. and Champagne A., *Nano Lett.*, **12** (2012) 4564.
[7] Rao A. M., Richter E., Bandow S., Chase B., Eklund P. C., Wiliams K. A., Fang S., Subbaswamy K. R., Menon M., Thess A., Smalley R. E., Dresselhaus G. and Dresselhaus M. S., *Science*, **275** (1997) 187.
[8] Fernandez I. R., Fangohr H. and Bhaskar A., *J. Phys.: Conf. Ser.*, **26** (2006) 131.
[9] Kahn D. and Lu J. P., *Phys. Rev. B*, **60** (1999) 6535.
[10] Ansari R., Ajori S. and Arash B., *Curr. Appl. Phys.*, **12** (2012) 707.
[11] Duan W. H., Wang C. M. and Zhang Y. Y., *J. Appl. Phys.*, **101** (2007) 024305.
[12] Zhang Y. Y., Wang C. M. and Tan V. B. C., *Adv. Appl. Math. Mech.*, **1** (2009) 89.
[13] Pine P., Yaish Y. E. and Adler J., *Phys. Rev. B*, **83** (2011) 155410; **84** (2011) 245409; **89** (2014) 115405.
[14] Yang J., Ke L. L. and Kitipornchai S., *Physica E*, **42** (2010) 1727.
[15] Shen Z. B., Sheng L. P., Li X. F. and Tang G. J., *Physica E*, **44** (2012) 1169.
[16] Mehdipour I., Moghadam A. E. and Mehdipour C., *Curr. Appl. Phys.*, **13** (2013) 1463.
[17] Papaconstantopoulos D. A., Mehl M. J., Erwin S. C. and Pederson M. R., *MRS Symp. Proc.*, **491** (1998) 221.
[18] Beu T. A., Onoe J. and Takeuchi K., *Eur. Phys. J. D*, **10** (2000) 391; **17** (2001) 205.
[19] Beu T. A. and Onoe J., *Phys. Rev. B*, **74** (2006) 195426.
[20] Beu T. A., Horváth L. and Ghişoiu I., *Phys. Rev. B*, **79** (2009) 054112.
[21] Beu T. A. and Jurjiu A., *Phys. Rev. B*, **83** (2011) 024103.